Influence of chondroitin sulfate glycan sulfation patterns on histochemical labeling of perineuronal nets: a comparative study of interregional distribution in human and mouse brain

Claudia Belliveau[1,2], Stéphanie Théberge[1,2], Stefanie Netto[1], Reza Rahimian[1], Gohar Fakhfouri[3], Clémentine Hosdey[1,2], Maria Antonietta Davoli[1], Aarun Hendrickson[4], Kathryn Hao[5], Bruno Giros[3], Gustavo Turecki[1,2,3], Kimberly M. Alonge[4,*] & Naguib Mechawar[1,2,3,*]

Affiliations

1 McGill Group for Suicide Studies, Douglas Mental Health University Institute, McGill University, Montreal, Qc, Canada

2 Integrated Program in Neuroscience, McGill University, Montreal, Qc, Canada

3 Department of Psychiatry, McGill University, Montreal, Qc, Canada

4 Department of Medicinal Chemistry, University of Washington, Seattle, USA

5 Health and Human Sciences, University of Southern California, Los Angeles, USA

(*) denotes shared authorship

Corresponding Authors

Naguib Mechawar, PhD

Douglas Mental Health University Institute

6875 Blvd LaSalle

Verdun, Qc

H4H 1R2

Canada

514-761-6131 x3365

naguib.mechawar@mcgill.ca

Kimberly Alonge, PhD

University of Washington

1959 NE Pacific Street

Box 357610

Seattle, WA 98195

United States

206-685-3543

kalonge@uw.edu

Keywords: Human, Mouse, Glycobiology, Extracellular Matrix, Adverse Childhood Experiences

Word count: 6281

Abstract

Perineuronal nets (PNNs) are a condensed subtype of extracellular matrix that form a net-like coverings around certain neurons in the brain. PNNs are primarily composed of chondroitin sulfate (CS) proteoglycans from the lectican family that consist of CS-glycosaminoglycan (CS-GAG) side chains attached to a core protein. CS disaccharides (CS-d) can exist in various isoforms with different sulfation patterns. Literature suggests that CS-d sulfation patterns can influence the function of PNNs as well as their labeling. This study was conducted to characterize such interregional CS-d sulfation pattern differences in adult human (N = 81) and mouse (N = 19) brains. Liquid chromatography tandem mass spectrometry was used to quantify five different CS-d sulfation patterns, which were then compared to immunolabeling of PNNs using *Wisteria Floribunda Lectin* (WFL) to identify CS-GAGs and anti-aggrecan to identify CS proteoglycans. In healthy brains, significant regional and species-specific differences in CS-d sulfation and single versus double-labeling pattern were identified. A secondary analysis to investigate how early-life stress (ELS) impacts these PNN features discovered that although ELS increases WFL+ PNN density, the CS-GAG sulfation code and single versus double PNN-labeling distributions remained unaffected in both species. These results underscore PNN complexity in traditional research, emphasizing the need to consider their heterogeneity in future experiments.

1. Introduction

Perineuronal nets (PNNs), first described by Camillo Golgi in 1893, are a condensed and specialized form of extracellular matrix (ECM) that surround the soma and proximal dendrites of various neurons in the central nervous system (Novak and Kaye, 2000). PNNs form preferentially around parvalbumin (PV) expressing inhibitory interneurons and, to a lesser extent, excitatory

neurons (Tanti et al., 2022). Comprising mainly chondroitin sulfate proteoglycans (CSPGs) from the lectican family (aggrecan, brevican, neurocan and versican), PNNs are synthesized by both the surrounding glia and neurons themselves exhibiting a highly organized mesh-like structure (**Figure 1A**) (Carulli et al., 2006; Celio et al., 1998; Schwartz and Domowicz, 2018; Tanti et al., 2022). The CSPGs are attached at their N-terminus through link proteins to a hyaluronan backbone that is secreted by hyaluronan synthase (HAS) located on the cell surface (Kwok et al., 2011) (**Figure 1B**). The CSPGs then bind to one another through Tenascin-R at their C-terminus, thus forming their characteristic PNN 'net-like' structures (Lundell et al., 2004).

PNN CSPGs consist of varying numbers of attached CS-GAG side chains (Schwartz and Domowicz, 2018). An additional layer of complexity is added by the CS-GAG length as well as the sulfate modifications to each CS-d unit (**Figure 1C**). Sulfate addition can occur on the C-4 and C-6 of the *N*-acetylgalactosamine (GalNAc), and C-2 of D-glucuronic acid (GlcA) that make up the CS disaccharide unit (Djerbal et al., 2017), which form five differentially sulfated CS isomers including non-sulfated (CS-O (0S)), mono-sulfated (CS-A (4S), -C (6S)) and di-sulfated (CS-D (2S6S), -E (4S6S)) variations. The relative abundances of these isomers incorporated into the PNNs constitute a sulfation code (Scarlett et al., 2022) that relates PNN composition to function (reviewed in (Djerbal et al., 2017)). For example, the ratio of 4-sulfation to 6-sulfation is an important regulator of brain development and aging. In the developing mouse brain (P0), 27.5% of CS isomers are comprised of 6-sulfation, which is permissive to neurocircuit plasticity and reorganization necessary for neurodevelopment. However, after the end of the critical period (P60), the 6-sulfation drops to 2.3% and instead 87.8% of CS isomers are comprised of 4-sulfation that matures PNN matrices, stabilizes neurocircuitry and limits plasticity of the underlying neurons (Miyata et al., 2012). Extracellular growth factors and proteins, including orthodenticle homeobox

protein 2 (Otx2) (Bernard and Prochiantz, 2016; Van't Spijker et al., 2019), interact with PNN CS-GAG chains and play a crucial role in the proper maturation of PV interneurons and the timing of the critical period of plasticity (Bernard and Prochiantz, 2016). For example, PNNs capture Otx2 through protein-glycan binding to the CS-E and CS-D variants, which also triggers maturation of the enmeshed neurons (Beurdeley et al., 2012). Notably, overexpression of chondroitin 6-sulfotransferase-1 (C6ST-1) in PV interneurons restricts the formation of stable PNNs and prevents binding of Otx2, resulting in aberrant maturation of PV interneurons and persistent cortical plasticity into adulthood (Miyata et al., 2012). Conversely, specific deletion of the chondroitin 4-sulfotransferase (C4ST-1) gene *Chst11* in mice leads to an augmentation of PNNs in CA2 of the hippocampus (Huang et al., 2023).

PNNs are also associated with the storage of long-term memories by limiting feedback inhibition from PV cells onto projection neurons (Shi et al., 2019). It is theorized that these extracellular nets preserve spatial information about synapses through the patterning of their holes (Tsien, 2013). Fear memories that persist into adulthood are actively preserved by PNNs in the amygdala, as illustrated by a reopening of the critical period and extinction of fear memory in adult mice in which local PNN CS-GAGs are enzymatically degraded using chondroitinaseABC (chABC) (Gogolla et al., 2009). Due to their protracted development and role in dampening the critical period of brain plasticity in humans and rodents, PNNs have attracted increasing attention in the fields of neurodevelopment (Wen et al., 2018), neurodegeneration (Lemarchant et al., 2016) and psychopathology (Browne et al., 2022; Carceller et al., 2023; Pantazopoulos and Berretta, 2016).

Early-life stress (ELS) coinciding with the critical period can alter PNN development in the rodent brain (Gildawie et al., 2020; Guadagno et al., 2021; Murthy et al., 2019; Santiago et al.,

2018) but the effects seem to be paradigm-specific, PNN detection method-specific and brain region-specific. We previously reported that PNN density, using WFL to label the CS-GAGs, is significantly increased in the ventromedial prefrontal cortex (vmPFC) of individuals who experienced child abuse compared to controls (Tanti et al., 2022). Building upon this, we hypothesize that not only are PNNs increased after child abuse, but their PNN CS-GAG sulfation patterning and consequently their function, are also affected. This study aimed to characterize PNN interregional differences in PNN sulfation coding and labeling patterns across three brain regions: the human vmPFC, entorhinal cortex (EC) and hippocampus (HPC), as well as their corresponding mouse equivalents (mPFC, EC, vHPC). Then, we explored the impact of ELS on these PNN characteristics in both species, recognizing the susceptibility of these brain regions to such influences (Murthy and Gould, 2020; Teicher et al., 2016).

2. Experimental procedures

Human post-mortem brain samples

Brain samples from a total of 81 individuals were obtained from the Douglas-Bell Canada Brain Bank (DBCBB; Montreal, Canada). In collaboration with Quebec's Coroner and the McGill Group for Suicide Studies, informed consent was obtained from the next of kin. Standardized psychological autopsies, medical records and Coroner reports were used to define cases and controls. Any presence of suspected neurodevelopmental, neurodegenerative, or neurological disorders in clinical files were basis for exclusion. In addition, proxy-based interviews with one or more informants that were closely acquainted with the deceased were used to create clinical vignettes with detailed medical and personal histories. Characterization of early-life histories were based on adapted Childhood Experience of Care and Abuse (CECA) interviews addressing the

experiences of sexual and physical abuse as well as neglect (Bifulco et al., 1994; Lutz et al., 2017). Reports of non-random major physical and/or sexual abuse during the first 15 years of life with a score of 1 or 2 on the CECA were considered as severe child abuse. A panel of clinicians reviewed and assessed all clinical vignettes to generate Diagnostic and Statistical Manual of Mental Disorders (DSM-IV) diagnostic criteria and classify the deceased as a case or control. Toxicology reports and medication prescriptions were also obtained. Three groups were compared in this study consisting of healthy individuals having died suddenly (CTRL; n=19), and depressed suicides with (DS-CA; n=33) or without (DS; n=30) a history of severe child abuse (characteristics detailed in **Table 1**).

Human tissue dissections and preparation

Expert staff at the DBCBB dissected 0.5cm-thick coronal sections from isopentane snap-frozen brain samples with the guidance of the human brain atlas (Juergen Mai, 2016). vmPFC samples were dissected from coronal sections equivalent to plate 3 (approximately -48mm from the center of the anterior commissure) of this atlas. Anterior HPC samples were obtained from sections equivalent to plate 37 of the atlas, by dissecting around hippocampal CA1-CA3, then between the EC and the parahippocampal gyrus. Samples were then fixed in 10% formalin for 24 h, followed by storage in 30% sucrose at 4°C until they sank. Tissue blocks were snap-frozen in isopentane at -35°C before being stored at -80°C until they were sectioned on a cryostat. 40µm-thick free-floating serial sections were stored in cryoprotectant at -20°C until use.

Early-life stress mouse model

Animal housing and experiments followed the Canadian Council on Animal Care (CCAC) guidelines, procedures were approved by the Animal Care Committee of the Douglas Research Center (Protocol number 5570) and all experiments were conducted in accordance with ARRIVE guidelines (Percie du Sert et al., 2020). 8-week-old male and female C57BL/6J mice were purchased from Charles Rivers, Wilmington, MA, USA. Mice were kept at the Douglas animal facility for at least a week before being bred by housing a single female with one male for one week. Females were monitored daily for the birth of pups. ELS was induced using the limited bedding and nesting paradigm, which causes fragmented maternal care from postnatal day (P)2 to P9, resulting in chronic stress in pups (Reemst et al., 2022; Rice et al., 2008). Briefly, at P2, in the ELS group, mother and litters were moved to cages with a small amount of corn husk bedding at the bottom and half of the standard amount of nesting material (2.5 x 5 cm piece of cotton nesting material) on top of a stainless-steel mesh which was placed 1 cm above the cage floor. Animals were left undisturbed until P9, when they were moved back to cages with regular housing conditions. CTRL cages were equipped with standard amounts of bedding and nesting material (5 x 5cm). Mice had access to standard chow and water *ad libitum* and were kept under a 12:12 h light-dark cycle. Animals were weaned at P21 and sacrificed at P70. Both male (CTRL = 5, ELS = 9) and female (CTRL = 5, ELS =5) mice were used in this study and no sex differences were observed.

Mouse brain preparation

At P70, mice were deeply anesthetized with an intraperitoneal injection of ketamine/xylazine (100/10 mg/kg, Sigma-Aldrich, St. Louis, MO, USA) and perfused transcardially with phosphate buffered saline (PBS) followed by 4% paraformaldehyde (PFA, pH 7.4, dissolved in PBS). Brains

were then extracted and post-fixed overnight in 4% PFA at 4 ºC and subsequently cryoprotected in 30% sucrose dissolved in PBS for 48 h at 4 ºC. Sunken brains were snap-frozen in isopentane at -35°C. Lastly, 35µm-thick serial coronal brain sections were collected free-floating and stored in cryoprotectant at -20°C until use.

Liquid chromatography tandem mass spectrometry

Six to ten serial sections from human vmPFC (CTRL = 14, DS = 16, DS-CA = 12), EC (CTRL = 7, DS = 21, DS-CA = 22), HPC (CTRL = 10, DS = 19, DS-CA = 20) or mouse (CTRL = 10, ELS = 9) mPFC, EC, vHPC samples were processed for liquid chromatography tandem mass spectrometry (LC-MS/MS) as previously described (Alonge et al., 2019; Logsdon et al., 2022). Briefly, samples were shipped from Montreal to Seattle in PBS + 0.02% sodium azide at 4°C. After manual dissections of the brain regions of interest (ROI), sections were washed thrice in Optima LC/MS-grade water and once in 50mM ammonium bicarbonate (pH 7.6) at room temperature (RT). Tissues were incubated with 50mU/mL of chABC (Sigma-Aldrich, C3667, Burlington, Massachusetts, USA) for 24 h at 37°C. The supernatant was filtered and lyophilized, then reconstituted in LC/MS-grade water for LC-MS/MS analysis.

LC-MS/MS + MRM quantification of isolated chondroitin sulfate disaccharides

Human and mouse CS isomers were subjected to quantification using a triple quadrupole (TQ) mass spectrometer equipped with an electrospray ion (ESI) source (Waters Xevo TQ-S) and operated in negative mode ionization as previously described (Alonge et al., 2019; Logsdon et al., 2022; Scarlett et al., 2022). Briefly, CS-disaccharides were resolved on porous graphite column (Hypercarb column; 2.1 × 50 mm, 3 µm; Thermo Fisher Scientific, Bothell, WA, USA) and LC-

MS/MS + MRM were performed using a Waters Acquity I-class ultra-performance liquid chromatographic system (UPLC) using the following MRM channels: CS-A (4S), *m/z* 458 > 300; CS-C (6S), *m/z* 458 > 282; CS-D (2S6S) and CS-E (4S6S), *m/z* 268 > 282; CS-O (0S), *m/z* 378 > 175. MassLynx software version 4.1 (Waters) was used to acquire and quantify all data using a modified peak area normalization function (Alonge et al., 2019). Each CS-disaccharide is shown as the relative percentage of all CS isomers within the sample. CS sulfation was computed using the weighed mean formula for the average number of sulfates (Avg#S) per CS-disaccharide (ΔCS):

$$Avg\#S/\Delta CS = \sum_{(i=1)}^{n} (x_i + w_i) \,/\, \sum_{(i=1)}^{n} w_i x_i = \#Sulfates(0-2)$$

$$w_i = percent\Delta CS$$

Immunolabelings, WFL staining, and image analysis

Free-floating sections of human or mouse brain were labeled for two PNN markers, the PNN CSPG aggrecan (anti-ACAN) and the PNN CS-GAGs (WFL), and co-localized with a neuronal marker (anti-NeuN) marker (**Table 2**). First, sections were rinsed thrice in PBS and then incubated overnight at 4°C under constant agitation with the appropriate antibody or lectin diluted in a blocking solution of PBS containing 0.2% Triton-X and 2% normal goat serum. Mouse tissues had an additional 1 h of blocking with 10% normal goat serum in PBS with 0.2% Triton-X before primary labeling. After overnight primary incubation, sections were rinsed thrice in PBS and incubated for 2h at RT with the appropriate fluorophore-conjugated secondary antibody or streptavidin (**Table 2**) diluted in the blocking solution. Next, tissues were rinsed and incubated with TrueBlack® (Biotium, #23007, Fremont, California, USA) for 80 seconds to remove

endogenous autofluorescence from lipofuscin and other cellular debris. Sections were then mounted on Superfrost charged slides and coverslipped with Vectashield mounting medium with DAPI (Vector Laboratories, H-1800, Newark, California, USA) and stored at 4°C until imaged on an Evident Scientific VS120 Slide Scanner at 20X magnification.

Image analysis was conducted with QuPath (Bankhead et al., 2017) version 0.3.2. Two to four ROIs spanning all cortical or subcortical layers were counted per human sample in the vmPFC (CTRL = 11, DS = 9, DS-CA = 9), EC (CTRL = 8, DS = 16, DS-CA = 14), HPC (CTRL = 8, DS = 15, DS-CA = 16) or mouse sample in the mPFC, EC, vHPC (CTRL = 10, ELS = 9). ROIs were manually investigated by a blinded researcher who manually classified PNNs as double positive (WFL+/ ACAN+) or solely labeled by WFL+ or ACAN+. A total of 30982 PNNs were classified in the human brain (14644 in vmPFC, 6920 in EC, 9418 in HPC) and 5902 in the mouse brain (1419 in mPFC, 2233 in EC, 2250 vHPC). PNN counts were normalized to 100 allowing for comparison between groups using percentage of total PNNs classified.

Statistical analyses

Statistical tests were conducted using Prism version 10 (GraphPad Software, Boston, Massachusetts, USA) and SPSS version 29.0 (IBM Corp, Armonk, New York, USA). Distribution and homogeneity of variances were assessed through Shapiro-Wilk and Levene's tests, respectively. Spearman's correlation was used to explore the relationship between dependent variables and covariates (age, PMI, pH, types of antidepressants and number of medications) (**Supplementary Figure 1**). Age exhibited a correlation with PNN labeling pattern, prompting the use of analysis of covariance (ANCOVA) to compare human labeling patterns. Analysis of variance (ANOVA) was used to compare sulfation pattern. Statistical tests were all two-sided with

a significance threshold of 0.05. Data are presented as mean ± standard error of the mean unless otherwise indicated.

3. Results

PNN sulfation code across the healthy brain

Human

To address confounding factors which may contribute to varied findings across brain regions in ELS research, we first used LC-MS/MS to characterize the CS-GAG sulfation code in healthy postmortem human brain tissue across three regions involved in emotion regulation and the threat response: the vmPFC, EC and HPC (Teicher et al., 2016). In psychiatrically healthy controls, mono-sulfated CS-A (4S) was the most abundant isomer in adult vmPFC (77.6%), EC (76.2%) and HPC (81.2%) compared to CS-C (6S) in the vmPFC (5.6%), EC (8.4%), and HPC (9.5%) (**Figure 2A**). This finding is consistent with developmental literature suggesting that CS-A replaces CS-C after the closure of the critical window of developmental neuroplasticity (Djerbal et al., 2017; Kitagawa et al., 1997; Miyata et al., 2012). Meanwhile, di-sulfated CS-D (between 2.0-3.1% of total CS isomers) and CS-E (1.1-1.2% of total CS isomers) were the least abundant in all three brain regions.

When testing for differences in sulfation patterning between human brain regions, we found significant variations between cortical and deep brain structures. The HPC (0.99 Avg#S/ΔCS) exhibited an increase in hypersulfation compared to the EC (0.92 Avg#S/ΔCS) and vmPFC (0.90 Avg#S/ΔCS) (**Figure 2B**). The hypersulfation observed in the HPC is driven by both the high abundance of mono- and di-sulfated isomers (CS-A, -C, -D), and decreased abundance of non-sulfated isomer (CS-O), specific to this brain region (**Figure 2C**). Meanwhile, the hyposulfation

observed in the vmPFC was dependent on the decreased abundance of sulfated CS-C and CS-D and increase in non-sulfated CS-O (**Figure 2C**). In comparison, the EC presented an intermediate Avg#S/ΔCS and abundance of non-sulfated, mono-sulfated and di-sulfated isomers when compared to the HPC and vmPFC (**Figure 2B-C**).

Mouse

To determine whether these region-specific differences in PNN CS-GAG sulfation profiling is conserved across species, we next determined the relative abundance of each CS isomers using LC-MS/MS in fixed, wild type mouse brain. Similar to humans (Figure 2), control mice showed CS-A as the most abundant isomer in the mPFC (70%), EC (73.9%), and vHPC (79.6%) (**Figure 3A**), while di-sulfated CS-E was the least abundant with 1.4% in the mPFC, 0.9% in the EC and 0.7% in the vHPC.

We also observed parallel differences in CS-GAG sulfation patterning between mouse brain regions, whereas the vHPC exhibited CS-GAG hypersulfation (0.94 Avg#S/ΔCS), both mPFC (0.85 Avg#S/ΔCS) and EC (0.85 Avg#S/ΔCS) were hyposulfated (**Figure 3B**). vHPC hypersulfation appeared to be driven by the high abundance of mono-sulfated isomers CS-A and CS-C and low abundance of non-sulfated CS-O (**Figure 3C**) compared to EC and mPFC. Unlike the human samples, the mPFC (17.6% of CS isomers) and EC (16.8% of CS isomers) exhibited similar CS-O sulfation levels.

Labeling patterns of PNNs across the healthy brain

Human

To characterize the labeling pattern of PNNs in relation to sulfation changes, tissues were co-labeled with both ACAN (PNN core protein) and WFL (PNN CS-GAGs). Matching previous reports, healthy human brain showed strong PNN labeling heterogeneity, including nets that appeared deglycosylated (WFL-/ACAN+) and those appearing glycosylated (WFL+/ACAN- and WFL+/ACAN+) (Härtig et al., 2022; Matthews et al., 2002; Miyata et al., 2018; Scarlett et al., 2022; Ueno et al., 2018) (**Figure 4A**). ACAN immunoreactivity was found to be associated with extracellular PNN formations but also within the cytoplasm of some cells (**Figure 4A cyan arrow**), as previously reported in neurons (Domowicz et al., 2000) as well as glia (Asher et al., 1995). Therefore, only ACAN labeling appearing as extracellular PNNs was included in further analyses (**Figure 4A yellow arrow**). We found that PNN heterogeneity varied significantly between brain regions, whereas the vmPFC exhibited the greatest amount of double labeled PNNs (48.3% WFL+/ACAN+) compared to the HPC (20.1%) and EC (12.7%) (**Figure 4B**). The EC presented the most WFL+/ACAN- labeling (66.8% of total PNNs) compared to HPC (25.7%) and vmPFC (28.3%), and the HPC exhibited the greatest amount of deglycosylated ACAN+ PNNs (54.2% WFL-/ACAN+) compared to the EC (20.5%) and vmPFC (23.4%) suggesting additional PNN core proteins may prevail in this region.

We then hypothesized that differences in PNN heterogeneity may be related to differences in PNN CS-GAG sulfation patterning unique to each brain region. By examining the total labeling of a marker (total ACAN labeling includes both the WFL-/ACAN+ and WFL+/ACAN+; total WFL labeling includes WFL+/ACAN- and WFL+/ACAN+), we observed large differences in total labeling between brain regions (**Figure 4C**). Compared to the vmPFC that showed equal abundance of ACAN (71.7%) vs WFL (76.6%) total PNN labeling, the EC exhibited a significantly higher total amount of WFL (79.4%) labeled PNNs compared to ACAN (33.2%) labeled PNNs. In

contrast, the HPC exhibited a significantly higher amount of ACAN (74.3%) labeled PNNs compared to WFL (45.8%) labeled PNNs (**Figure 4C**).

Mouse

To investigate whether labeling pattern of PNNs is conserved across species, healthy mouse brain was also co-labeled with WFL and ACAN (**Figure 5A**). Surprisingly, the labeling pattern of PNNs is highly dissimilar between species. In the mouse mPFC and EC, 94.7% and 92.3%, of all PNNs were labeled as WFL+/ACAN- (**Figure 5B**). Nearly all other PNNs in these brain areas were found to be double positive for WFL+/ACAN+ (5.5-7.1%), while very few PNNs in the mPFC and EC labeled as WFL-/ACAN+ (0-0.6%, **Figure 5C**). The specificity of the ACAN antibody was demonstrated by intracellular ACAN immunoreactivity (as observed in human samples and not considered for analysis) as well as by the abundance of ACAN+ PNNs in the adjacent brain regions within the same coronal sections (**Figure 5C**). In contrast, the vHPC displayed more heterogeneity in PNN labeling with all three populations being present: 12.5% WFL-/ACAN+, 39.5% WFL+/ACAN- and 47.9% WFL+/ACAN+ (**Figure 5B**). Once again, the mPFC and EC appeared to display much higher levels of glycosylation than the vHPC, as seen in humans.

When comparing the total labeling of ACAN (WFL-/ACAN+, WFL+/ACAN+) or WFL (WFL+/ACAN+, WFL+/ACAN-) between regions, we observed a similar labeling pattern of WFL across the brain in mice and humans, but ACAN was differentially dispersed (**Figure 5D**). In the mPFC and EC, 99.4-100% of PNNs were labeled with WFL, while in the vHPC only 87.5% of PNNs were labeled. In contrast, the vHPC exhibited 60.5% of PNNs labeled with ACAN while the mPFC and EC only had 5.4-7.7% of PNNs stained with ACAN respectively.

ELS influences PNN abundance but not sulfation code

Human

Although we previously reported an increase in density of WFL+ PNNs in the vmPFC of individuals who died by suicide during a depressive episode with a history of child abuse (Tanti et al., 2022), there was no significant difference in the relative abundance of CS isomers associated with suicide (DS) or abuse (DS-CA) in any of the three regions analysed compared to controls (CTRL) (**Figure 6A-C**). Additionally, the labeling pattern landscape did not vary with abuse throughout the brain (**Figure 6D-F**).

Mouse

Initially, to validate our mouse model of ELS, we examined the density of WFL+ PNNs in the mPFC. Replicating our previously published human data (Tanti et al., 2022) we found that there are significantly more WFL+ PNNs in the mPFC of ELS mice (N = 9) compared to CTRL mice (N = 10) (**Figure 6G**). Although, PNN CS-GAG abundance appeared elevated, ELS did not influence the underlying CS-GAG sulfation code (**Figure 6H-J**) or labeling pattern (**Figure 6K-M**) in any of the three mouse brain regions investigated. These results suggest that ELS only has a long-lasting effect on PNN CS-GAG abundance and not composition, an observation we found conserved between species.

4. Discussion

We observed and characterized for the first time vastly different relative abundances of CS-d isomers and PNN labeling patterns between brain regions across species, shedding new

translational light on the intricate foundations of PNN composition. We initially predicted there would be a higher amount of double labeled PNNs (WFL+/ACAN+) in all brain regions across species based on evidence suggesting that ACAN is necessary for PNN formation *in vitro* (Giamanco et al., 2010) and in vivo (Rowlands et al., 2018). Although most studies investigating changes in PNN abundance are conducted using WFL as a universal PNN marker and a widely accepted histochemical visualization method, WFL was recently shown to preferentially bind to non-sulfated CS-d (CS-O) (Nadanaka et al., 2020). Although we did not observe a significant correlation between labeling pattern and sulfation score *per se* (**Supplementary Figure 1**), we did find that brain regions with the highest levels of non-sulfated CS-O also exhibited the strongest PNN labeling with WFL. In both healthy human and mouse brain, the (v)mPFC and EC had the most glycosylation (total WFL labeling) and the most CS-O. In comparison, the (v)HPC had the least glycosylation and lowest percentages of CS-O. These findings are consistent with previous research showing increased CS-O content in the somatosensory cortex correlated to elevated WFL+ PNN labeling in P45 mice when compared to the adjacent dorsal hippocampus (Scarlett et al., 2022). Interestingly, the hippocampus is also the brain region with the highest amount of CS-A which has been shown to be useful for creating a healthy niche for neural stem cells through its ability to bind basic fibroblast growth factor (Djerbal et al., 2017). Overall, these findings highlight the limitations of using WFL as a pan-PNN labeling marker.

This study emphasizes the importance of using multiple markers in order to accurately represent the degree of regional PNN diversity throughout the brain. It was originally thought that PNNs would double label when combining WFL labeling and immunohistochemistry with anti-CSPG antibodies (Härtig et al., 1994). However, more recent evidence suggests that WFL does not always co-label PNNs detected with anti-CSPG antibodies (Härtig et al., 2022; Matthews et al.,

2002; Miyata et al., 2018; Scarlett et al., 2022; Ueno et al., 2018), including anti-aggrecan (ACAN). Moreover, rodent literature shows that different CSPG antibodies bind to different portions of the large proteoglycan such that three different antibodies for ACAN (Cat-301, Cat-315 and Cat-316) bind selectively to this target at unique sites. Nevertheless, their labeling pattern is completely different depending on the brain region and glycosylation pattern of the CSPG (Matthews et al., 2002). The adult human cortex, specifically Brodmann area 6, expresses all forms of ACAN isoforms (Virgintino et al., 2009) albeit to different extent throughout the cortical neuronal layers and enmesh different cell types. In our study, Cat-301, which labels the core protein itself, was the anti-ACAN antibody used to label human brain samples. In contrast, Cat-316 binds selectively to non-sulfated CS-GAG on ACAN and labels more similarly to WFL (Matthews et al., 2002), thus producing a different landscape of ACAN PNN labeling throughout the brain. The antibody used in the mouse brain for this study also binds to the core protein itself, as apparent by the molecular weight reported by the manufacturer (**Table 2**).

The unique composition of PNNs in different brain regions and species, as seen here and by others (Lensjø et al., 2017; Matthews et al., 2002), suggests region-specific roles in regulating plasticity and memory processes. Literature indicates that PNN formation may be dependent on neuronal activity (Devienne et al., 2021; Kind et al., 2012; McRae et al., 2010; Rowlands et al., 2018) implying that regions with more labeling are highly active compared to regions with less labeling. Interestingly, this phenomenon has been observed using both WFL and ACAN to visualize the nets, although none of the indicated studies examined both markers at the same time. Given PNN heterogeneity in both CS core proteins and associated CS-GAG sulfation patterns, future studies should explore their composition at the single-cell level, as this should shed light on

the functional consequences of varied sulfation patterns on different neuronal subtypes across brain regions and species.

The present study also investigated the long-lasting impact of early-life adversity on PNN heterogeneity and composition in the (v)mPFC, EC and (v)HPC of adult human and mouse brain. Using an ELS mouse model of limited bedding and nesting from P2-9 (Reemst et al., 2022), we found that WFL+ PNNs are increased in the mPFC of P70 male and female mice compared to controls (**Figure 6**). Moreover, our findings elucidate that PNN sulfation code and labeling pattern are undisturbed in adult human and mouse brains that have experienced early-life adversity. We cannot exclude, however, that this code was altered earlier in life during and/or shortly after the ELS but then restored thereafter. Biochemical composition changes of PNNs are not solely restricted to the critical period of plasticity early in life. For example, glia are becoming increasingly involved in the production, maintenance and degradation of cerebral PNNs (Crapser et al., 2021) in adult mice (Venturino et al., 2021) and humans (Crapser et al., 2020) in health and disease. Glia are also known to produce and secrete C4ST-1 (Bhattacharyya et al., 2015) and C6ST-1 (Properzi et al., 2005), main regulators of CS-GAG sulfation. It will be important to further investigate how cerebral PNNs are affected by early-life adversity, given the rich body of research highlighting the long-lasting impact of ELS on WFL+ PNNs across various paradigms and brain regions in different species (Gildawie et al., 2020; Guadagno et al., 2021; Murthy et al., 2019; Santiago et al., 2018; Tanti et al., 2022).

This study is not without limitations. Firstly, we examined bulk tissue for LC-MS/MS and not individual PNNs and acknowledge that both interstitial and PNN CS-GAGs may have been included in our analyses. However, interstitial ECM has 9X more hyaluronan sulfate than CS, and CS are highly condensed into PNNs (Deepa et al., 2006), so we are confident in the readout of the

sulfation code as a representation of changes in PNN CS-GAGs. We also acknowledge that more detailed, multi-point longitudinal studies in animal models of ELS should be conducted to further investigate temporal changes in sulfation code and resultant labeling.

Figures

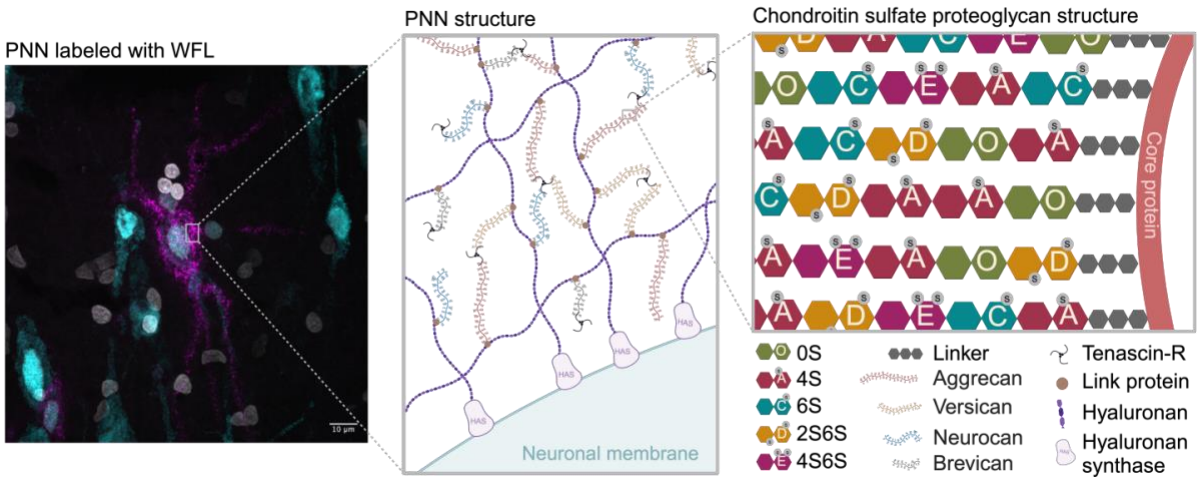

Figure 1: Perineuronal net composition and structure **A** Representative micrograph of a WFL+ PNN surrounding the soma and proximal dendrites of a neuron in the postmortem human entorhinal cortex. Imaged at 60X on Evident Scientific FV1200 Confocal, scale bar 10µm **B** PNNs are primarily composed of CSPGs from the lectican family (aggrecan, versican, neurocan and brevican) intricately linked to a hyaluronan backbone synthesized on the cell surface through link proteins. CSPGs are attached to each other through Tenascin-R, resulting in a distinctive net-like structure known as the PNN. **C** CSPGs have varying number of CS-GAG side chains made up of CS-disaccharides that exist in different isomers based on sulfate groups added to either C-4 or C-6 of the GalNAc or C-2 of GlcA including non-sulfated CS-O (0S), mono-sulfated CS-A (4S), -C (6S) and di-sulfated CS-D (2S6S), -E (4S6S). WFL: Wisteria Floribunda Lectin, PNN: perineuronal net, CSPGs: chondroitin sulfate proteoglycans, CS-GAG: chondroitin sulfate glycosaminoglycan, GalNAc: N-acetylgalactosamine, GlcA: D-glucuronic acid, HAS: hyaluronan synthase

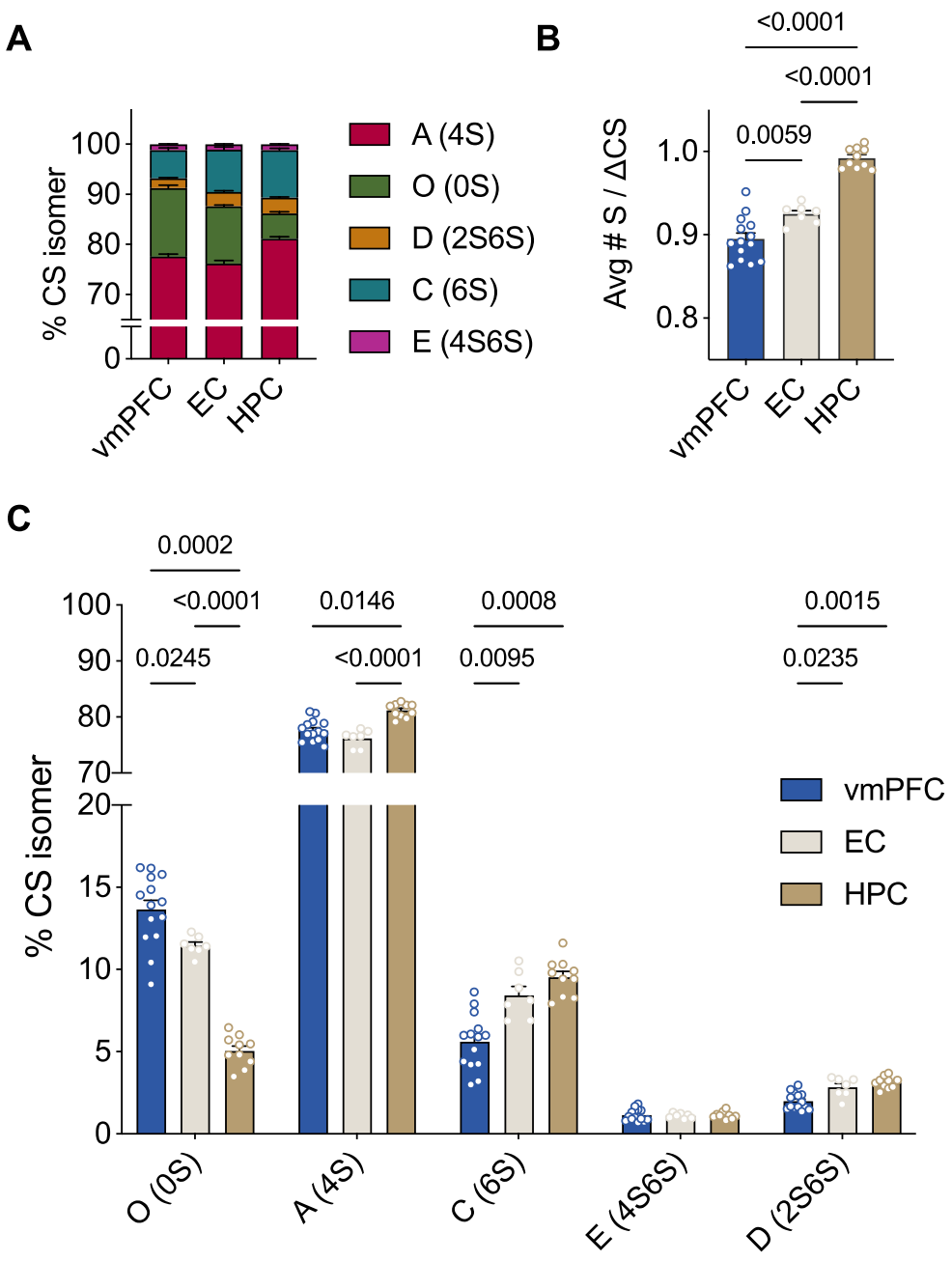

Figure 2: CS-GAG sulfation code varies significantly between brain regions in healthy postmortem human brain **A** Comparison of the relative abundance of each CS isomer in the control vmPFC (N = 14), EC (N = 7) and HPC (N = 10) measured by LC-MS/MS **B** The HPC is the most hypersulfated region on average while the vmPFC is the most hyposulfated region (Welch's ANOVA: $W(2,18) = 101$, $P < 0.0001$, followed by Dunnett's test) **C** Hypersulfation in the HPC is

driven by mono-sulfated CS-A, -C and di-sulfated CS-D, while hyposulfation is driven by high abundance of CS-O in the vmPFC. Each isomer is expressed differently in each brain region except for isomer CS-E (4S6S) (ANOVA: isomer effect: $F(2,61) = 20074$, $P < 0.0001$; region effect: $F(0.1, 10) = 5.478e-20$, $P > 0.9999$; isomer x region: $F(2,43) = 54.23$, $P < 0.0001$, followed by Tukey's test). Avg#S/ΔCS: average number of sulfates per chondroitin sulfate disaccharide, CS-GAG: chondroitin sulfate glycosaminoglycan, vmPFC: ventromedial prefrontal cortex, EC: entorhinal cortex, HPC: hippocampus, LC-MS/MS: liquid chromatography tandem mass spectrometry, ANOVA: analysis of variance.

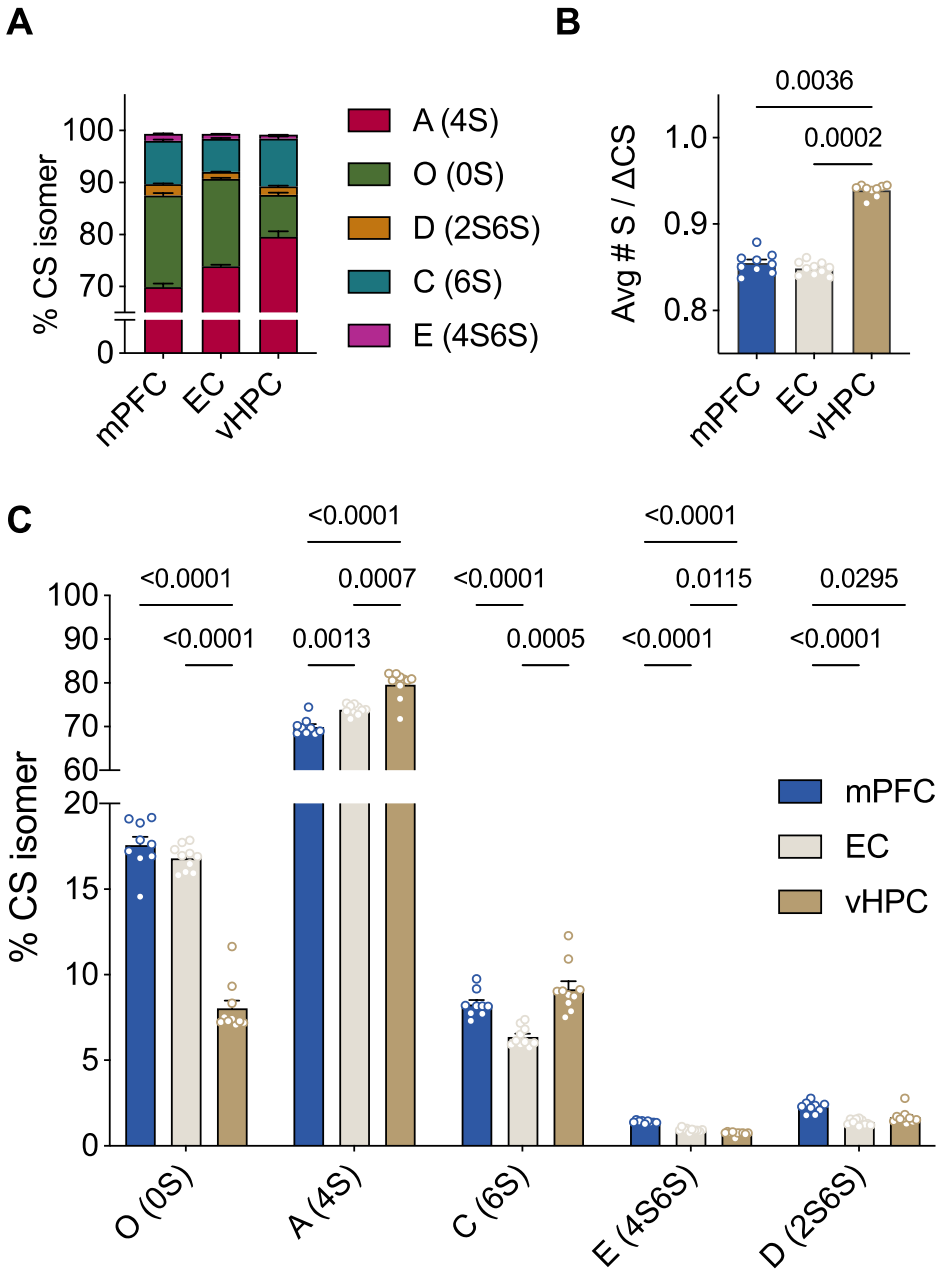

Figure 3: CS-GAG sulfation code is generally conserved between species in the healthy brain **A** Comparison of the relative abundance of each CS isomer in the control mPFC, EC and vHPC of mouse (N = 10) brain measured by LC-MS/MS **B** Like human brain, the mouse vHPC is hypersulfated compared to both the EC and mPFC, however, in this species the mPFC and EC do not differ in average sulfation (Kruskal-Wallis test: P = 0.0001, followed by Dunn's test) **C** All

CS-isomers are expressed in significantly different abundances across the healthy mouse brain (ANOVA: isomer effect: $F(1,11) = 13984$, $P < 0.0001$; region effect: $F(1, 12) = 0.01896$, $P = 0.940$; isomer x region : $F(2, 16) = 97.49$, $P < 0.0001$, followed by Tukey's test). Avg#S/ΔCS: average number of sulfates per chondroitin sulfate disaccharide, CS-GAG: chondroitin sulfate glycosaminoglycan, LC-MS/MS: liquid chromatography tandem mass spectrometry, mPFC: medial prefrontal cortex, EC: entorhinal cortex, vHPC: ventral hippocampus, ANOVA: analysis of variance.

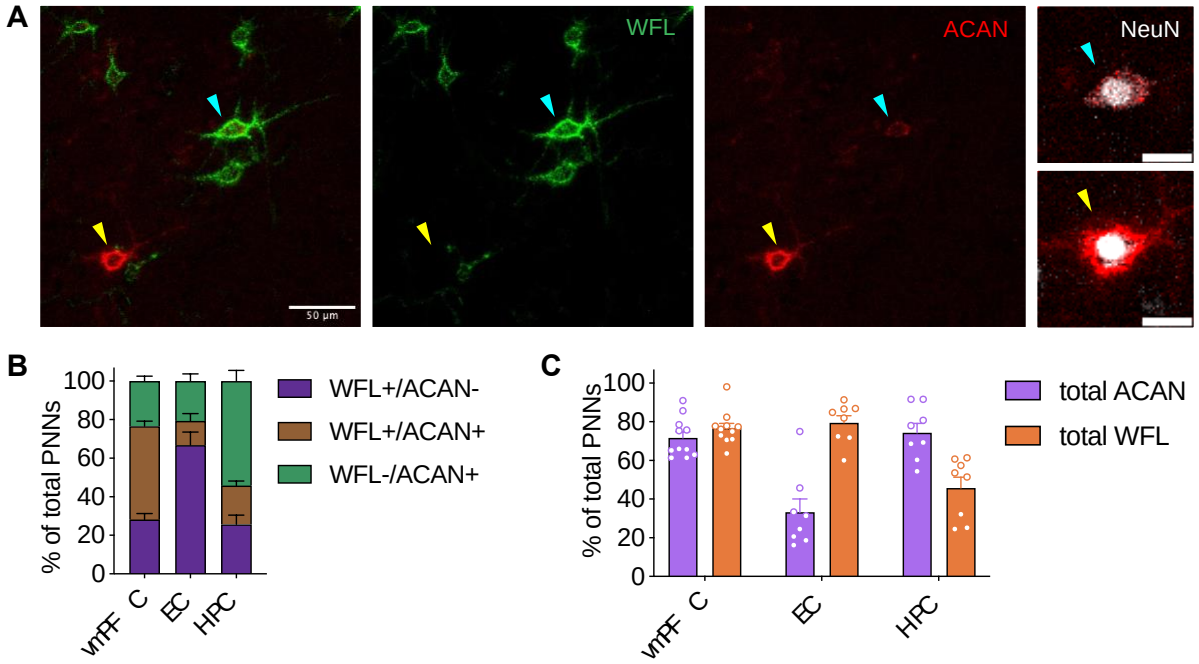

Figure 4: Immunohistochemical staining of healthy human brain reveals heterogeneity in perineuronal net labeling that differs between brain regions **A** PNN populations in the vmPFC (N = 11), EC (N = 8) and HPC (N = 8) display either single (WFL+/ACAN- or WFL-/ACAN+) or double (WFL+/ACAN-) labeling. ACAN staining can be found intracellularly (cyan arrow) or in the distinctive pattern of an extracellular PNN (yellow arrow), only the latter was counted in this study. Imaged at 20X on Evident Scientific FV1200 Confocal, scale bar 50µm (left) and 20µm (right) **B** Comparison of the labeling patterning between the different brain regions investigated.

C Total ACAN (WFL+/ACAN+ and WFL-/ACAN+) and total WFL (WFL+/ACAN- and WFL+/ACAN+) labeling can be found in different amounts depending on the brain region. Within the vmPFC the two markers label similarly, while WFL prevails in the EC and ACAN predominates in the HPC. WFL: Wisteria Floribunda Lectin, ACAN: anti-aggrecan core protein, NeuN: anti-neuronal nuclei, vmPFC: ventromedial prefrontal cortex, EC: entorhinal cortex, HPC: hippocampus.

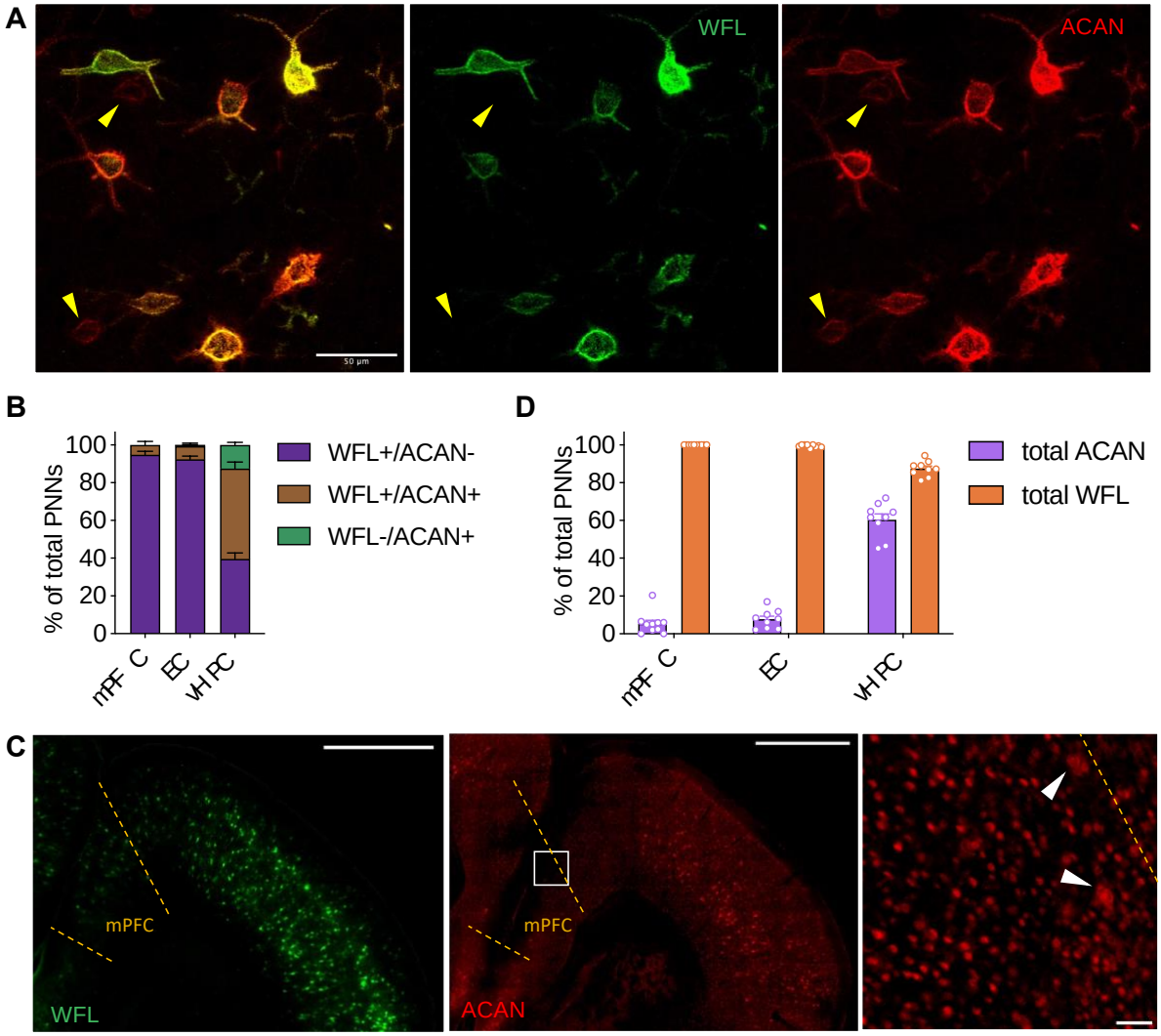

Figure 5: Perineuronal net labeling is highly dissimilar between species **A** Immunohistochemical labeling of PNNs in the vHPC displays WFL+/ACAN+ nets, WFL-/ACAN+ (yellow arrow) and

WFL+/ACAN- (not displayed) populations. Imaged at 20X on Evident Scientific FV1200 Confocal, scale bar 50µm **B** Unlike the human samples, barely any PNNs were labeled solely by WFL-/ACAN+ in control mouse mPFC and EC (N=10), while the vHPC expressed all three categories of labeling **C** Representative image of a coronal section of mouse brain with the mPFC delineated. Although there is barely any PNN labeling by ACAN in the mPFC (white arrows), ACAN can be seen intracellularly, as in humans. Imaged at 20x on Evident Scientific VS120 Slide Scanner, scale bar 1 mm (left) and 50µm (right). **D** Examination of total WFL or ACAN labeling within brain regions reveals that WFL labels many more PNNs in all brain regions examined. WFL: Wisteria Floribunda Lectin, ACAN: anti-aggrecan core protein, mPFC: medial prefrontal cortex, EC: entorhinal cortex, vHPC: ventral hippocampus.

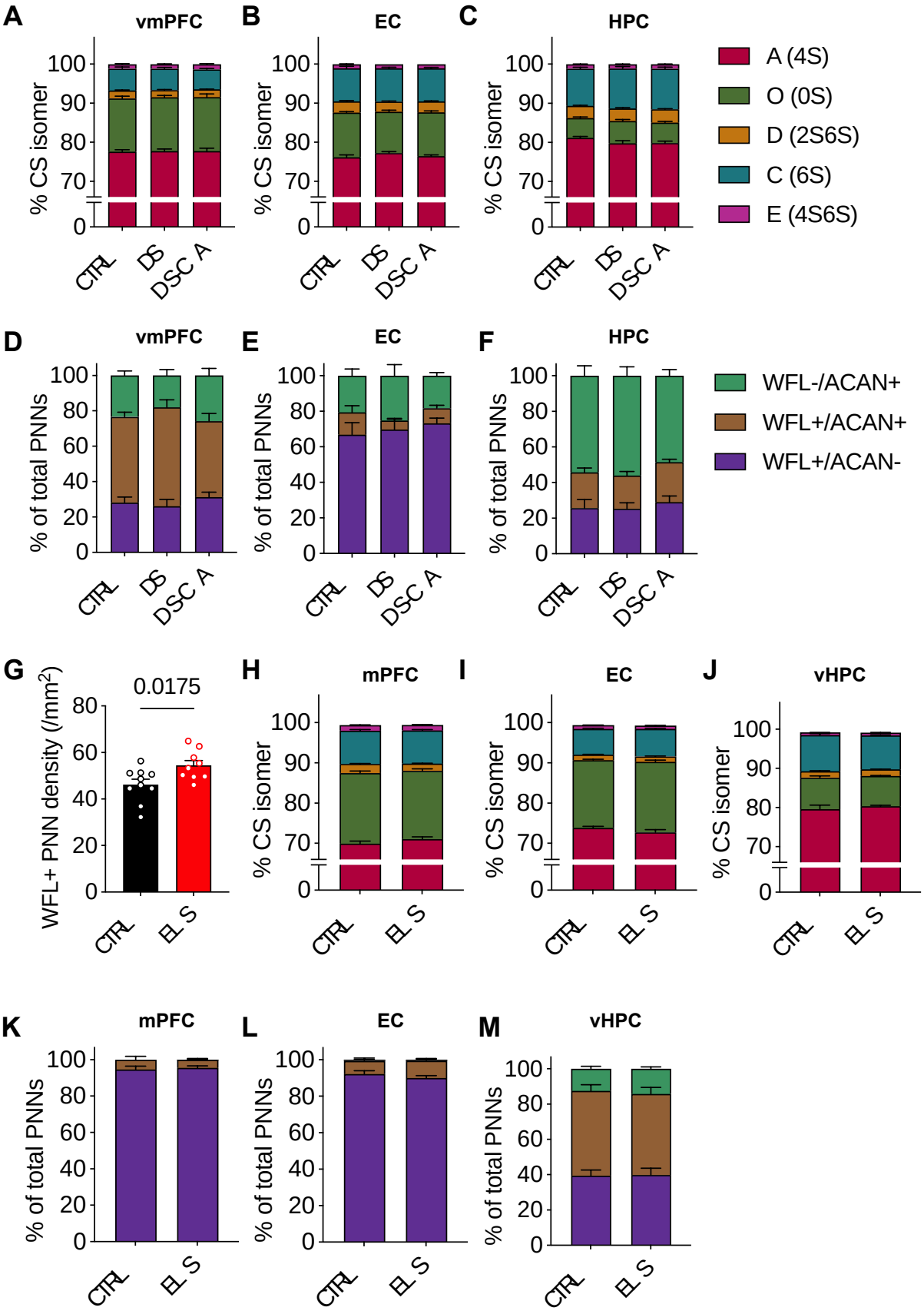
A
vmPFC
B
EC
C
HPC
% CS isomer
100
90
80
70
0
CTRL
DS
DSC A
A (4S)
O (0S)
D (2S6S)
C (6S)
E (4S6S)
D
vmPFC
E
EC
F
HPC
% of total PNNs
100
80
60
40
20
0
WFL-/ACAN+
WFL+/ACAN+
WFL+/ACAN-
G
WFL+ PNN density (/mm2)
0.0175
80
60
40
20
0
CTRL
ES
H
mPFC
I
EC
J
vHPC
% CS isomer
K
mPFC
L
EC
M
vHPC
% of total PNNs

Figure 6: Perineuronal net sulfation code and labeling pattern are preserved after the experience of early-life stress in both human and mouse brain A-C Within each human brain region CS-GAG sulfation code is unaffected by depression, suicide (DS) and child abuse (DS-CA) when compared to controls (CTRL) (ANOVA: vmPFC group x isomer: $F(3,67) = 0.132$, $P = 0.929$; EC group x isomer: $F(3,13) = 1.448$, $P = 0.275$; HPC group x isomer: $F(2,6) = 1.210$, $P = 0.372$) D-F Although we previously reported a significant increase in WFL+ PNNs in the vmPFC, overall labeling pattern is conserved between groups in all brain regions examined (ANCOVA with age as covariate: vmPFC group x labeling: $F(4,50) = 2.104$, $P = 0.094$; EC group x labeling: $F(3,38) = 0.471$, $P = 0.65$; HPC group x labeling: $F(3,47) = 0.152$, $P = 0.961$) G Limited bedding and nesting from P2-9 is associated with a significant increase in WFL+ PNNS in the mPFC of adult mice ($N = 9$) compared to control ($N = 10$) (Welch's t-test: $P = 0.0175$) H-J Within each mouse brain region CS-GAG sulfation code is unaffected by early-life stress (ANOVA: mPFC group x isomer: $F(1,21) = 1.761$, $P = 0.200$; EC group x isomer: $F(1,9) = 5.029$, $P = 0.464$ although does not pass Bonferroni's multiple comparisons test; vHPC group x isomer: $F(1,22) = 0.683$, $P = 0.424$) K-M Although we report an increase in WFL+ PNNs in the mPFC of mice, the overall landscape of PNN labeling by WFL and ACAN is resilient to ELS (ANOVA: mPFC group x labeling: $F(2,34) = 0.248$, $P = 0.782$; EC group x labeling: $F(2,32) = 1.33$, $P = 0.279$; vHPC group x labeling: $F(2, 32) = 0.140$, $P = 0.870$). CTRL: psychiatrically healthy control, DS: depressed suicide, DS-CA: depressed suicide with a history of child abuse, CS-GAG: chondroitin sulfate glycosaminoglycan, WFL: Wisteria Floribunda Lectin, ACAN: anti-aggrecan core protein, vmPFC: ventromedial prefrontal cortex, EC: entorhinal cortex, HPC: hippocampus, ANCOVA: analysis of covariance, mPFC: medial prefrontal cortex, EC: entorhinal cortex, vHPC: ventral hippocampus, ANOVA: analysis of variance.

Tables

Table 1: Group characteristics			
	CTRL	**DS**	**DS-CA**
N = 81	18	30	33
Axis 1 diagnosis	0	MDD (25); DD-NOS (5)	MDD (26); DD-NOS (7)
Age (years) (P = 0.06)	48.1 ± 20.2	50.4 ± 12.5	41.5 ± 14.6
Sex (M/F)	13/5	25/5	22/11
PMI (h) (P = 0.14)	41.1 ± 25.0	54.0 ± 29.0	56.9 ± 27.7
Tissue pH (P = 0.99)	6.5 ± 0.3	6.5 ± 0.4	6.5 ± 0.4
Substance dependence	0	8	8
Last 3 months medication	Sedative hypnotics (1)	Classic antidepressants (4); Benzodiazepines (9); SNRI (4); SSRI (6); Antipsychotic (3); TCA (2); Antimanic (1); Opioid (1)	Classic antidepressants (2); Benzodiazepines (6); SNRI (3); SSRI (7); Antipsychotic (3); TCA (1); Antimanic (1); Opioid (2); NASSA (2); SARI (1); Anticonvulsant (2); GABA analog (1)

Table 2: Specific labeling					
Abbreviation	**Primary**	**Labels**	**Target species**	**Product**	**Fluorophore conjugated-secondary**
Human samples					
WFL	Biotinylated Wisteria Floribunda Lectin	Perineuronal nets	Human	Vector Laboratories, B-1355, 1:2500	Alexa 488-Streptavidin, Jackson ImmunoResearch, 016-540-084, 1:500
NeuN	Anti-neuronal nuclei	Neurons	Human	Abcam, ab104225, 1:1000	DyLight-594 anti-rabbit, Jackson ImmunoResearch, 111-515-144, 1:500
ACAN	Anti-chondroitin sulfate proteoglycan brain core protein (Cat-301)	Perineuronal nets	Human	Millipore, MAB5284, 1:500	Alexa-647 anti-mouse, Jackson ImmunoResearch, 115-605-146, 1:500
Mouse samples					
WFA	Biotinylated Wisteria Floribunda Agglutin	Perineuronal nets	Mouse	Vector Laboratories, B-1355, 1:1500	Cy3-Streptavidin, Jackson ImmunoResearch, 016-160-084, 1:500
NeuN	Anti-neuronal nuclei	Neurons	Mouse	Millipore, MAB377, 1:500	Alexa-647 anti-mouse, Jackson ImmunoResearch, 115-605-146, 1:500
ACAN	Anti-aggrecan	Perineuronal nets	Mouse	Millipore, AB1031, 1:100	Alexa-488 anti-rabbit. Jackson ImmunoResearch, 111-485-144, 1:500

References

Alonge, K.M., Logsdon, A.F., Murphree, T.A., Banks, W.A., Keene, C.D., Edgar, J.S., Whittington, D., Schwartz, M.W., Guttman, M., 2019. Quantitative analysis of chondroitin sulfate disaccharides from human and rodent fixed brain tissue by electrospray ionization-tandem mass spectrometry. Glycobiology 29, 847-860.

Asher, R.A., Scheibe, R.J., Keiser, H.D., Bignami, A., 1995. On the existence of a cartilage-like proteoglycan and link proteins in the central nervous system. Glia 13, 294-308.

Bankhead, P., Loughrey, M.B., Fernández, J.A., Dombrowski, Y., McArt, D.G., Dunne, P.D., McQuaid, S., Gray, R.T., Murray, L.J., Coleman, H.G., James, J.A., Salto-Tellez, M., Hamilton, P.W., 2017. QuPath: Open source software for digital pathology image analysis. Sci Rep 7, 16878.

Bernard, C., Prochiantz, A., 2016. Otx2-PNN Interaction to Regulate Cortical Plasticity. Neural Plast 2016, 7931693.

Beurdeley, M., Spatazza, J., Lee, H.H., Sugiyama, S., Bernard, C., Di Nardo, A.A., Hensch, T.K., Prochiantz, A., 2012. Otx2 binding to perineuronal nets persistently regulates plasticity in the mature visual cortex. J Neurosci 32, 9429-9437.

Bhattacharyya, S., Zhang, X., Feferman, L., Johnson, D., Tortella, F.C., Guizzetti, M., Tobacman, J.K., 2015. Decline in arylsulfatase B and Increase in chondroitin 4-sulfotransferase combine to increase chondroitin 4-sulfate in traumatic brain injury. J Neurochem 134, 728-739.

Bifulco, A., Brown, G.W., Harris, T.O., 1994. Childhood Experience of Care and Abuse (CECA): a retrospective interview measure. J Child Psychol Psychiatry 35, 1419-1435.

Browne, C.A., Conant, K., Lasek, A.W., Nacher, J., 2022. Editorial: Perineuronal Nets as Therapeutic Targets for the Treatment of Neuropsychiatric Disorders. Front Synaptic Neurosci 14, 889800.

Carceller, H., Gramuntell, Y., Klimczak, P., Nacher, J., 2023. Perineuronal Nets: Subtle Structures with Large Implications. Neuroscientist 29, 569-590.

Carulli, D., Rhodes, K.E., Brown, D.J., Bonnert, T.P., Pollack, S.J., Oliver, K., Strata, P., Fawcett, J.W., 2006. Composition of perineuronal nets in the adult rat cerebellum and the cellular origin of their components. J Comp Neurol 494, 559-577.

Celio, M.R., Spreafico, R., De Biasi, S., Vitellaro-Zuccarello, L., 1998. Perineuronal nets: past and present. Trends Neurosci 21, 510-515.

Crapser, J.D., Arreola, M.A., Tsourmas, K.I., Green, K.N., 2021. Microglia as hackers of the matrix: sculpting synapses and the extracellular space. Cell Mol Immunol 18, 2472-2488.

Crapser, J.D., Spangenberg, E.E., Barahona, R.A., Arreola, M.A., Hohsfield, L.A., Green, K.N., 2020. Microglia facilitate loss of perineuronal nets in the Alzheimer's disease brain. EBioMedicine 58, 102919.

Deepa, S.S., Carulli, D., Galtrey, C., Rhodes, K., Fukuda, J., Mikami, T., Sugahara, K., Fawcett, J.W., 2006. Composition of perineuronal net extracellular matrix in rat brain: a different disaccharide composition for the net-associated proteoglycans. J Biol Chem 281, 17789-17800.

Devienne, G., Picaud, S., Cohen, I., Piquet, J., Tricoire, L., Testa, D., Di Nardo, A.A., Rossier, J., Cauli, B., Lambolez, B., 2021. Regulation of perineuronal nets in the adult cortex by the activity of the cortical network. J Neurosci 41, 5779-5790.

Djerbal, L., Lortat-Jacob, H., Kwok, J., 2017. Chondroitin sulfates and their binding molecules in the central nervous system. Glycoconj J 34, 363-376.

Domowicz, M., Mangoura, D., Schwartz, N.B., 2000. Cell specific-chondroitin sulfate proteoglycan expression during CNS morphogenesis in the chick embryo. Int J Dev Neurosci 18, 629-641.

Giamanco, K.A., Morawski, M., Matthews, R.T., 2010. Perineuronal net formation and structure in aggrecan knockout mice. Neuroscience 170, 1314-1327.

Gildawie, K.R., Honeycutt, J.A., Brenhouse, H.C., 2020. Region-specific Effects of Maternal Separation on Perineuronal Net and Parvalbumin-expressing Interneuron Formation in Male and Female Rats. Neuroscience 428, 23-37.

Gogolla, N., Caroni, P., Lüthi, A., Herry, C., 2009. Perineuronal nets protect fear memories from erasure. Science 325, 1258-1261.

Guadagno, A., Belliveau, C., Mechawar, N., Walker, C.D., 2021. Effects of Early Life Stress on the Developing Basolateral Amygdala-Prefrontal Cortex Circuit: The Emerging Role of Local Inhibition and Perineuronal Nets. Front Hum Neurosci 15, 669120.

Härtig, W., Brauer, K., Bigl, V., Brückner, G., 1994. Chondroitin sulfate proteoglycan-immunoreactivity of lectin-labeled perineuronal nets around parvalbumin-containing neurons. Brain Res 635, 307-311.

Härtig, W., Meinicke, A., Michalski, D., Schob, S., Jäger, C., 2022. Update on Perineuronal Net Staining With Wisteria floribunda Agglutinin (WFA). Front Integr Neurosci 16, 851988.

Huang, H., Joffrin, A.M., Zhao, Y., Miller, G.M., Zhang, G.C., Oka, Y., Hsieh-Wilson, L.C., 2023. Chondroitin 4-O-sulfation regulates hippocampal perineuronal nets and social memory. Proc Natl Acad Sci U S A 120, e2301312120.

Juergen Mai, M.M., George Paxinos, 2016. Atlas of the Human Brain. 4th Ed. Elseiver.

Kind, P.C., Sengpiel, F., Beaver, C.J., Crocker-Buque, A., Kelly, G.M., Matthews, R.T., Mitchell, D.E., 2012. The Development and Activity-Dependent Expression of Aggrecan in the Cat Visual Cortex. Cerebral Cortex 23, 349-360.

Kitagawa, H., Tsutsumi, K., Tone, Y., Sugahara, K., 1997. Developmental regulation of the sulfation profile of chondroitin sulfate chains in the chicken embryo brain. J Biol Chem 272, 31377-31381.

Kwok, J.C., Dick, G., Wang, D., Fawcett, J.W., 2011. Extracellular matrix and perineuronal nets in CNS repair. Dev Neurobiol 71, 1073-1089.

Lemarchant, S., Wojciechowski, S., Koistinaho, J., 2016. Perineuronal nets in neurodegeneration. Oncotarget 7, 78224-78225.

Lensjø, K.K., Christensen, A.C., Tennøe, S., Fyhn, M., Hafting, T., 2017. Differential Expression and Cell-Type Specificity of Perineuronal Nets in Hippocampus, Medial Entorhinal Cortex, and Visual Cortex Examined in the Rat and Mouse. eNeuro 4.

Logsdon, A.F., Francis, K.L., Richardson, N.E., Hu, S.J., Faber, C.L., Phan, B.A., Nguyen, V., Setthavongsack, N., Banks, W.A., Woltjer, R.L., Keene, C.D., Latimer, C.S., Schwartz, M.W., Scarlett, J.M., Alonge, K.M., 2022. Decoding perineuronal net glycan sulfation patterns in the Alzheimer's disease brain. Alzheimers Dement 18, 942-954.

Lundell, A., Olin, A.I., Mörgelin, M., al-Karadaghi, S., Aspberg, A., Logan, D.T., 2004. Structural basis for interactions between tenascins and lectican C-type lectin domains: evidence for a crosslinking role for tenascins. Structure 12, 1495-1506.

Lutz, P.E., Tanti, A., Gasecka, A., Barnett-Burns, S., Kim, J.J., Zhou, Y., Chen, G.G., Wakid, M., Shaw, M., Almeida, D., Chay, M.A., Yang, J., Larivière, V., M'Boutchou, M.N., van Kempen, L.C., Yerko, V., Prud'homme, J., Davoli, M.A., Vaillancourt, K., Théroux, J.F., Bramoullé, A., Zhang, T.Y., Meaney, M.J., Ernst, C., Côté, D., Mechawar, N., Turecki, G., 2017. Association of a History of Child Abuse With Impaired Myelination in the Anterior Cingulate Cortex: Convergent Epigenetic, Transcriptional, and Morphological Evidence. Am J Psychiatry 174, 1185-1194.

Matthews, R.T., Kelly, G.M., Zerillo, C.A., Gray, G., Tiemeyer, M., Hockfield, S., 2002. Aggrecan glycoforms contribute to the molecular heterogeneity of perineuronal nets. J Neurosci 22, 7536-7547.

McRae, P.A., Baranov, E., Sarode, S., Brooks-Kayal, A.R., Porter, B.E., 2010. Aggrecan expression, a component of the inhibitory interneuron perineuronal net, is altered following an early-life seizure. Neurobiology of Disease 39, 439-448.

Miyata, S., Komatsu, Y., Yoshimura, Y., Taya, C., Kitagawa, H., 2012. Persistent cortical plasticity by upregulation of chondroitin 6-sulfation. Nat Neurosci 15, 414-422, s411-412.

Miyata, S., Nadanaka, S., Igarashi, M., Kitagawa, H., 2018. Structural Variation of Chondroitin Sulfate Chains Contributes to the Molecular Heterogeneity of Perineuronal Nets. Front Integr Neurosci 12, 3.

Murthy, S., Gould, E., 2020. How Early Life Adversity Influences Defensive Circuitry. Trends Neurosci 43, 200-212.

Murthy, S., Kane, G.A., Katchur, N.J., Lara Mejia, P.S., Obiofuma, G., Buschman, T.J., McEwen, B.S., Gould, E., 2019. Perineuronal Nets, Inhibitory Interneurons, and Anxiety-Related Ventral Hippocampal Neuronal Oscillations Are Altered by Early Life Adversity. Biol Psychiatry 85, 1011-1020.

Nadanaka, S., Miyata, S., Yaqiang, B., Tamura, J.I., Habuchi, O., Kitagawa, H., 2020. Reconsideration of the Semaphorin-3A Binding Motif Found in Chondroitin Sulfate Using Galnac4s-6st-Knockout Mice. Biomolecules 10.

Novak, U., Kaye, A.H., 2000. Extracellular matrix and the brain: components and function. J Clin Neurosci 7, 280-290.

Pantazopoulos, H., Berretta, S., 2016. In Sickness and in Health: Perineuronal Nets and Synaptic Plasticity in Psychiatric Disorders. Neural Plast 2016, 9847696.

Percie du Sert, N., Hurst, V., Ahluwalia, A., Alam, S., Avey, M.T., Baker, M., Browne, W.J., Clark, A., Cuthill, I.C., Dirnagl, U., Emerson, M., Garner, P., Holgate, S.T., Howells, D.W., Karp, N.A., Lazic, S.E., Lidster, K., MacCallum, C.J., Macleod, M., Pearl, E.J., Petersen, O.H., Rawle, F., Reynolds, P., Rooney, K., Sena, E.S., Silberberg, S.D., Steckler, T., Würbel, H., 2020. The ARRIVE guidelines 2.0: Updated guidelines for reporting animal research. PLOS Biology 18, e3000410.

Properzi, F., Carulli, D., Asher, R.A., Muir, E., Camargo, L.M., van Kuppevelt, T.H., ten Dam, G.B., Furukawa, Y., Mikami, T., Sugahara, K., Toida, T., Geller, H.M., Fawcett, J.W., 2005. Chondroitin 6-sulphate synthesis is up-regulated in injured CNS, induced by injury-related cytokines and enhanced in axon-growth inhibitory glia. Eur J Neurosci 21, 378-390.

Reemst, K., Kracht, L., Kotah, J.M., Rahimian, R., van Irsen, A.A.S., Congrains Sotomayor, G., Verboon, L.N., Brouwer, N., Simard, S., Turecki, G., Mechawar, N., Kooistra, S.M., Eggen, B.J.L., Korosi, A., 2022. Early-life stress lastingly impacts microglial transcriptome and function under basal and immune-challenged conditions. Translational Psychiatry 12, 507.

Rice, C.J., Sandman, C.A., Lenjavi, M.R., Baram, T.Z., 2008. A novel mouse model for acute and long-lasting consequences of early life stress. Endocrinology 149, 4892-4900.

Rowlands, D., Lensjø, K.K., Dinh, T., Yang, S., Andrews, M.R., Hafting, T., Fyhn, M., Fawcett, J.W., Dick, G., 2018. Aggrecan Directs Extracellular Matrix-Mediated Neuronal Plasticity. J Neurosci 38, 10102-10113.

Santiago, A.N., Lim, K.Y., Opendak, M., Sullivan, R.M., Aoki, C., 2018. Early life trauma increases threat response of peri-weaning rats, reduction of axo-somatic synapses formed by parvalbumin cells and perineuronal net in the basolateral nucleus of amygdala. J Comp Neurol 526, 2647-2664.

Scarlett, J.M., Hu, S.J., Alonge, K.M., 2022. The "Loss" of Perineuronal Nets in Alzheimer's Disease: Missing or Hiding in Plain Sight? Front Integr Neurosci 16, 896400.

Schwartz, N.B., Domowicz, M.S., 2018. Proteoglycans in brain development and pathogenesis. FEBS Lett 592, 3791-3805.

Shi, W., Wei, X., Wang, X., Du, S., Liu, W., Song, J., Wang, Y., 2019. Perineuronal nets protect long-term memory by limiting activity-dependent inhibition from parvalbumin interneurons. Proc Natl Acad Sci U S A 116, 27063-27073.

Tanti, A., Belliveau, C., Nagy, C., Maitra, M., Denux, F., Perlman, K., Chen, F., Mpai, R., Canonne, C., Théberge, S., McFarquhar, A., Davoli, M.A., Belzung, C., Turecki, G., Mechawar, N., 2022. Child abuse associates with increased recruitment of perineuronal nets in the ventromedial prefrontal cortex: a possible implication of oligodendrocyte progenitor cells. Molecular Psychiatry 27, 1552-1561.

Teicher, M.H., Samson, J.A., Anderson, C.M., Ohashi, K., 2016. The effects of childhood maltreatment on brain structure, function and connectivity. Nat Rev Neurosci 17, 652-666.

Tsien, R.Y., 2013. Very long-term memories may be stored in the pattern of holes in the perineuronal net. Proc Natl Acad Sci U S A 110, 12456-12461.

Ueno, H., Fujii, K., Suemitsu, S., Murakami, S., Kitamura, N., Wani, K., Aoki, S., Okamoto, M., Ishihara, T., Takao, K., 2018. Expression of aggrecan components in perineuronal nets in the mouse cerebral cortex. IBRO Rep 4, 22-37.

Van't Spijker, H.M., Rowlands, D., Rossier, J., Haenzi, B., Fawcett, J.W., Kwok, J.C.F., 2019. Neuronal Pentraxin 2 Binds PNNs and Enhances PNN Formation. Neural Plast 2019, 6804575.

Venturino, A., Schulz, R., De Jesús-Cortés, H., Maes, M.E., Nagy, B., Reilly-Andújar, F., Colombo, G., Cubero, R.J.A., Schoot Uiterkamp, F.E., Bear, M.F., Siegert, S., 2021. Microglia enable mature perineuronal nets disassembly upon anesthetic ketamine exposure or 60-Hz light entrainment in the healthy brain. Cell Rep 36, 109313.

Virgintino, D., Perissinotto, D., Girolamo, F., Mucignat, M.T., Montanini, L., Errede, M., Kaneiwa, T., Yamada, S., Sugahara, K., Roncali, L., Perris, R., 2009. Differential distribution of aggrecan isoforms in perineuronal nets of the human cerebral cortex. J Cell Mol Med 13, 3151-3173.

Wen, T.H., Binder, D.K., Ethell, I.M., Razak, K.A., 2018. The Perineuronal 'Safety' Net? Perineuronal Net Abnormalities in Neurological Disorders. Front Mol Neurosci 11, 270.